Experimental observation and interpretation of magnetic polariton modes in FeF_2

1997 J. Phys.: Condens. Matter 9 7233

(http://iopscience.iop.org/0953-8984/9/34/013)

J. Phys.: Condens. Matter **9** (1997) 7233–7247. Printed in the UK PII: S0953-8984(97)83598-9

Experimental observation and interpretation of magnetic polariton modes in FeF_2

M R F Jensen†, S A Feiven†, T J Parker† and R E Camley‡

† Department of Physics, University of Essex, Colchester CO4 3SQ, UK

‡ Department of Physics, University of Colorado at Colorado Springs, CO 80933-7150, USA

Received 22 April 1997

Abstract. We demonstrate how the interpretation of high-resolution far-infrared reflectivity and ATR spectra allows the mapping out of experimentally determined dispersion curves for the antiferromagnet FeF_2. The dispersion curves clearly summarize the relationship between frequency and wave vector of magnetic polaritons, and show the position of the bulk and surface modes and surface resonances in zero, low and relatively strong applied fields. Surface resonances which exist only in the presence of damping are identified. In addition we show how far-infrared measurements can provide independent measurements of material parameters such as the exchange and anisotropy fields and the sublattice magnetization.

1. Introduction

The study of magnetic excitations has proved to be a key tool in the understanding of the properties of layered, metallic ferromagnetic-based structures. Fundamental properties of the structure including interfacial exchange and anisotropies have been obtained largely through Brillouin light scattering experiments [1–3], which is the appropriate tool for measuring spin waves with frequencies in the 10–40 GHz range.

Magnetic spin waves in antiferromagnets, in contrast, have frequencies which usually lie in the range of 100 GHz to 2 THz. Inelastic neutron scattering experiments [4] are often used to provide information about the magnetic spin waves, but such experiments generally do not provide information about surface excitations. The natural tool therefore for studying excitations in this frequency range is far-infrared spectroscopy [5]. There are many far-infrared studies of phonon–polaritons and plasmon–polaritons reported in the literature [6, 7]. Such works have given detailed information on the properties of semiconductor superlattices, including effective masses of charge carriers and surface charge densities [8].

There are two major differences between the properties of phonon– and plasmon–polaritons and the magnetic polaritons that we will discuss in this paper. First, the non-magnetic excitations have features which are fairly broad in frequency—for example, reststrahl bands may extend over 20 cm^{-1}. The reststrahl bands in antiferromagnets are significantly narrower, of the order of 0.4 cm^{-1} in width. Since the surface waves are to be found in the reststrahl bands, this requires a system with very high frequency resolution. Secondly, the magnetic excitations have a key signature of non-reciprocity [9] not present in other systems. Here reversing the direction of propagation (or equivalently reversing the applied field) produces dramatic changes in the reflectivity or in the attenuated total reflection (ATR) signal. This is generally associated with a non-reciprocity of the magnetic surface polariton itself.

0953-8984/97/347233+15$19.50

Earlier experimental studies of magnetic polaritons were carried out by using a laser operating at a single frequency [10, 11]. The magnetic excitation to be observed is then measured by changing the external magnetic field which shifts the magnetic excitation through the laser frequency. The laser brings the immediate advantage of the high resolution necessary to see the narrow magnetic excitations, but also has the obvious disadvantage that information at only one frequency is obtained.

Recently, a series of experiments studying magnetic polaritons [12–14] on FeF_2 with a high-resolution Fourier transform spectrometer operating in the far infrared [12, 13] have been reported. The initial work concentrated on oblique-angle reflectivity measurements, while the most recent ATR techniques led to the first observation of a magnetic surface polariton on an antiferromagnet [14].

The work presented here significantly extends the earlier experimental studies and this paper gives a thorough account of the results presented recently as a brief report [15]. Using a combination of ATR and reflectivity we map out complete dispersion curves for both bulk and surface polaritons. In particular we are able to show that the group velocity for surface polaritons in the presence of an external magnetic field is strongly non-reciprocal, thus confirming theoretical predictions made over a decade ago. In addition, and in contrast to earlier work, we show how values for the individual fields that govern the spin-wave excitations, the exchange field H_E and the anisotropy field H_A, can be individually obtained from far-infrared measurements alone. Earlier studies required additional measurements of the transverse magnetic susceptibility [16]. Finally we show that the concept of a surface resonance, where a surface excitation exists inside a bulk band as a mode with a finite lifetime, can be used to explain the significant non-reciprocity of the reflectivity seen in the frequency range where bulk excitations exist.

2. Experimental mapping out of dispersion curves

In this section we experimentally obtain the dispersion relations governing bulk and surface magnetic polaritons on a uniaxial antiferromagnet. This work demonstrates how high-resolution spectroscopic measurements probing both bulk modes and surface modes can be qualitatively and quantitatively explained and all of the observed features identified.

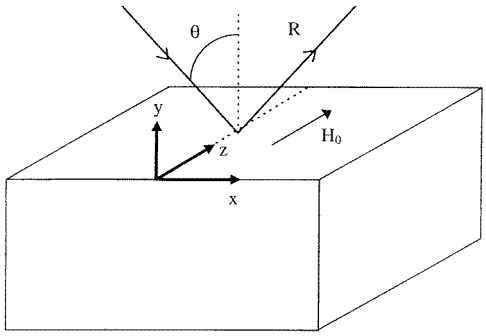

Figure 1. An illustration of the Voigt geometry.

The measurements were obtained using a unique high-resolution Fourier transform spectrometer operating in the far infrared. The sample, in this case FeF_2, is held inside a liquid helium cryostat between the poles of a 7 T superconducting magnet. We consider

here the Voigt geometry (figure 1) where radiation incident in the xy-plane strikes the sample occupying the space $y < 0$ with the reflecting surface in the xz-plane. The applied field is parallel to the sample surface in the z-direction. The results reported here were obtained with the sample easy axis either parallel or transverse to the applied field. Only linearly polarized light (s- or p-polarized) is considered. For the reflectivity measurements, the angle of incidence is limited to $\theta = \pm 45^\circ$.

Since the previous reported observation of the magnetic surface polariton using the technique of ATR [14], the attainable experimental resolution has been increased from 0.06 cm^{-1} to 0.02 cm^{-1} to resolve the surface mode from the bulk bands, and the fabrication of a new Si ATR prism to permit measurements at an angle of 30° has virtually overcome the problem of interference fringes encountered with a 45° prism.

Theoretical dispersion curves calculated for antiferromagnets have in a large number of publications been used to describe and summarize the interactions which take place between incident electromagnetic radiation and magnetic excitations in the sample [16–20]. The dispersion curves (frequency versus wave vector) are closely related to the experimental reflection spectra in that each spectrum is in effect the result of probing the dispersion curves along a specific scan line which is determined by the scattering geometry. In ATR the far-infrared radiation first strikes a Si prism which is placed ~10–20 μm above the surface of the antiferromagnet. An evanescent wave in the gap below the base of the prism is created when the angle of incidence, ϕ, is greater than the critical angle, $\phi_c = \sin^{-1}(\varepsilon_p^{-1/2})$. This wave has a wave vector given by $k_\parallel = \pm(\omega/c)\varepsilon_p^{1/2}\sin\phi$, which defines the ATR scan lines seen later on the dispersion curves. This also defines the reflectivity scan line for which $\varepsilon_p = 1$. If the wave vector and frequency of the external radiation match those of the bulk or surface excitation, coupling is possible and a reduction in the reflectivity is observed. Three different silicon prisms, $\varepsilon_p = 11.56$, with angles of incidence of 30°, 45° and 50°, were used along with the reflectivity measurements to give four $\boldsymbol{k}$ vectors at a given frequency. A reversal of the external magnetic field is equivalent to reversing the sign of $\boldsymbol{k}$, thus giving a total of eight wave vectors at a given frequency.

We wish to produce experimental dispersion curves for various values of H_0 so we need to be able to identify the origin of the observed features by consideration of the line shape. The shape of the spectrum depends on the interaction of the external radiation with the electromagnetic modes of the antiferromagnet. In general one would expect a broad region in frequency of reduced reflectivity at the frequency of the bulk bands. Any sharp dips, where the reflectivity drops below the level of the bulk bands, indicate the presence of surface excitations, i.e. surface modes or surface resonances. The surface resonances will be discussed in more detail in a later section. In the reststrahl regions the measured reflectivity rises sharply and in theory in the absence of damping would tend to unity. From previous publications [17, 18] we expect to see two bulk bands for zero external field, and with an external field present we expect to see an additional bulk band in the gap between the upper and lower bands seen for $H_0 = 0$ T.

In figures 2–5 we show representative reflectivity and ATR spectra. These spectra have been carefully analysed and the results of these and other spectra are plotted against the theoretical dispersion curves in figure 6. Figures 2 and 3 (top and bottom panels) show experimental (thin line) and theoretical (thick line) oblique-incidence reflectivity curves for an applied external field of $H_0 = 0$ T and ± 0.3 T respectively. The shape of the spectra allows identification of the various modes. We consider first the zero-field case. The spectrum initially shows a nearly flat reduced reflectivity indicative of a broad bulk band up to about 52 cm^{-1}. The dip just above 52 cm^{-1} is identifiable as a surface excitation due

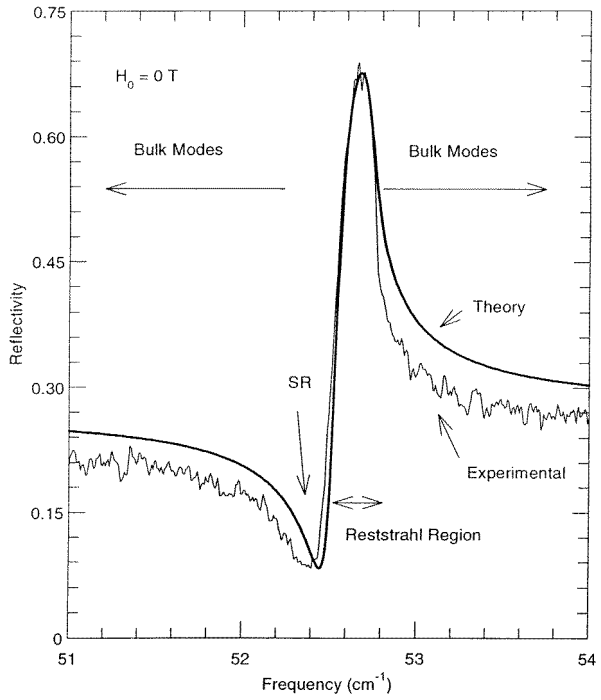

Figure 2. Experimental (thin solid line) and theoretical (thick line) reflectivity spectra of FeF_2 measured with zero applied field with the easy axis aligned along the z-axis. $T = 1.7$ K and the resolution is 0.02 cm^{-1}.

to the stronger coupling and the much sharper line shape. To compare with the dispersion curves, traverse up either of the 45° reflectivity scan lines, A or A′, in figure 6(a) and the frequency of the sharp dip is where the scan lines cross the surface feature within the bulk region. Just past this point the dramatic increase in the reflectivity marks the end of the bulk band and the beginning of the reststrahl region. Immediately past the reststrahl region the reduction in the measured reflectivity to a nearly flat region is caused, as expected, by the broad band of bulk polaritons. This allows us to identify the edge of the bulk band. From the spectrum there is a clear difference between the surface excitation and the bulk excitations, and we have clearly identified the sharp dip as a surface feature. The theoretical fit to the experimental data is calculated using previously published parameters [14]. The parameters used are the exchange field, $H_E = 53.3$ T, the anisotropy field, $H_A = 19.7$ T, and the sublattice magnetization, $M_S = 560$ G. The gyromagnetic ratio, γ, has been changed very slightly from 1.05 cm^{-1} T^{-1} to 1.0525 cm^{-1} T^{-1} to produce a better fit. The theoretical calculations include an anisotropic g-factor with $g_\perp$ about 10% smaller than $g_\parallel$ [16]. This inclusion was necessary to produce a close match between theory and experiment using the above parameters. As can be seen, the theory and the experiment are in good agreement.

When a relatively weak field ($H_0 = \pm 0.3$ T) is applied the spectra are more complicated. This is due to the appearance of the additional bulk band in the reststrahl region between the upper and lower bulk bands. We expect the reflectivity of the surface modes for propagation in the $+\boldsymbol{k}$ direction to be different to that for the $-\boldsymbol{k}$ direction, so it is necessary to probe both sides of the dispersion curves. This, of course, is easily done simply by reversing the applied field. Reading figure 3 (top and bottom panels) from the

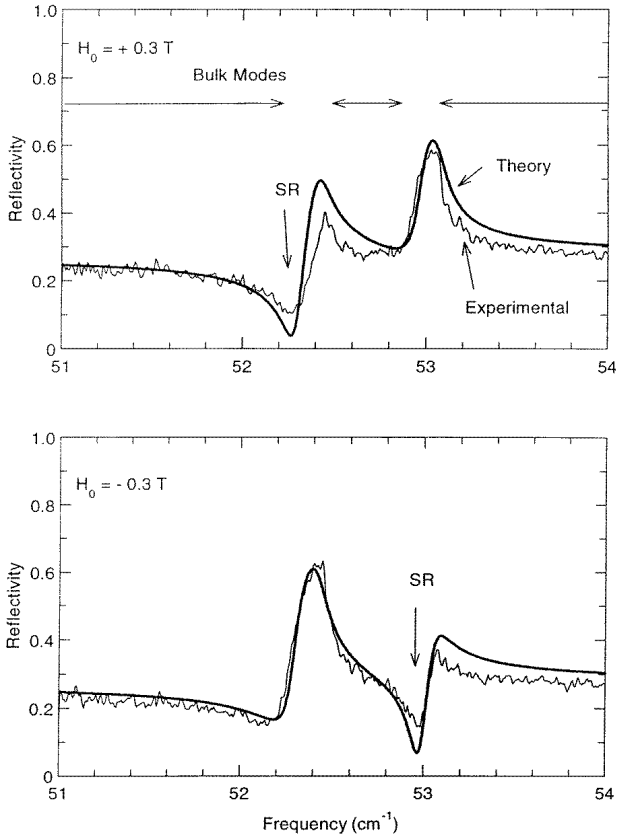

Figure 3. Experimental (thin line) and theoretical (thick line) reflectivity spectra of FeF_2 with the easy axis aligned along the z-axis. $T = 1.7$ K and the resolution is 0.02 cm^{-1}; (top panel) $H_0 = +0.3$ T and (bottom panel) $H_0 = -0.3$ T.

lower-frequency end and comparing this to the reflectivity scan lines A and A′ in figure 6(b) the first feature identified is a broad bulk region with a nearly flat but low reflectivity. This is, as expected, observed for both $+H_0$ and $-H_0$ and is where the scan lines pass through the lower bulk region. The reflectivity at just over 52 cm^{-1} then changes dramatically for $+H_0$, but remains virtually the same for $-H_0$. Unlike the -0.3 T spectrum the $+0.3$ T spectrum clearly has a much sharper surface dip which on the dispersion curve (figure 6(b)) is where the scan line is seen to cross the surface feature present only on the $+\boldsymbol{k}$ side of the dispersion curve. The equivalent curve for the $-H_0$ spectrum simply shows a continuation of the broad bulk region. The end of the lower bulk region and start of the reststrahl region is marked by the dramatic increase in reflectivity due to the gap between the lower and middle bulk bands, and the upper edge of the middle bulk band is clear from the rapid increase in the reflectivity following the bulk interaction. This is in good agreement with the dispersion curves as the scan lines pass through the bulk bands and the reststrahl regions. Again near the upper edge of the middle band the spectra are highly non-reciprocal for $+H_0$ and $-H_0$. Just below 53 cm^{-1} only the spectrum for $-H_0$ shows a sharp dip where the scan line for $-\boldsymbol{k}$ crosses the surface feature which is only seen on one side of the dispersion curve. Past the narrow reststrahl region of high reflectivity the reflectivity again drops for

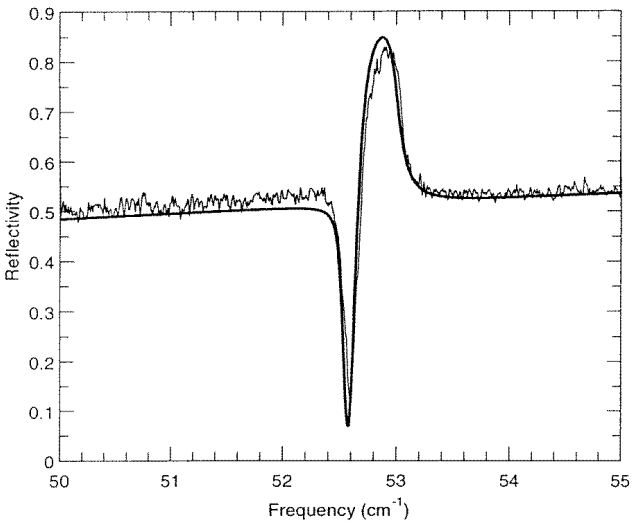

Figure 4. Experimental (thin line) and theoretical (thick line) ATR spectra of FeF_2 measured with zero applied field. $\phi = 30^\circ$, $T = 1.7$ K and the resolution is 0.02 cm^{-1}.

both $+H_0$ and $-H_0$ due to the upper bulk band. Again the theoretical curves calculated using the above parameters are in complete agreement with the experimental data.

Figure 4 shows the observed ATR measurement in the absence of an applied field. The angle of incidence is 30° and the ATR gap between the prism and the sample is around 17 μm. The interpretation of the spectrum is similar to that of the zero-field curve; however, it is clear that the surface dip is now observed at a slightly higher frequency, in agreement with the theoretical calculations seen in figure 6(a), scan lines B and B′. Comparison of the reflectivity and the ATR spectra reveals that the edges of the bulk bands have also shifted slightly due to the enhanced wave vector introduced by the prism. This is also clearly visible on the dispersion curve. Again since the dispersion curve (figure 6(a)) is reciprocal for propagation in the $+\boldsymbol{k}$ and $-\boldsymbol{k}$ directions, the spectrum can be understood with reference to either of the 30° ATR scan lines.

The ATR spectra obtained with an angle of incidence of 30° and an applied field of ± 0.3 T are shown in figure 5 which can be understood with reference to scan lines B and B′ in figure 6(b). The lower bulk region is identified from the broad reduction in the reflectivity as before. The level of the measured reflectivity for bulk interactions is different from that in the reflectivity spectra due to the introduction of the ATR gap which reduces the coupling to the bulk modes. The edge of the lower bulk band is easily visible for $H_0 = +0.3$ T. Here the surface mode and the lower bulk modes are clearly resolved and we see an increase in the reflectivity at around 52 cm^{-1} due to the gap between the lower bulk region and the surface mode. Reversing the field brings the surface mode to a lower frequency which is also clear from the dispersion curve. It is still in the reststrahl region, but due to magnon damping it is now too close to the lower bulk region to be resolved; however, it is now well away from the middle bulk band which as a result can be fully resolved. The non-reciprocity of the two spectra is very striking since following the 30° ATR scan lines up in frequency the positions on the frequency scale at which the scan lines cross the surface features are very different for propagation in the $+\boldsymbol{k}$ and $-\boldsymbol{k}$ directions. For example, at the surface mode frequency for $+H_0$ the observed reflectivity differs by about 80% for the spectra

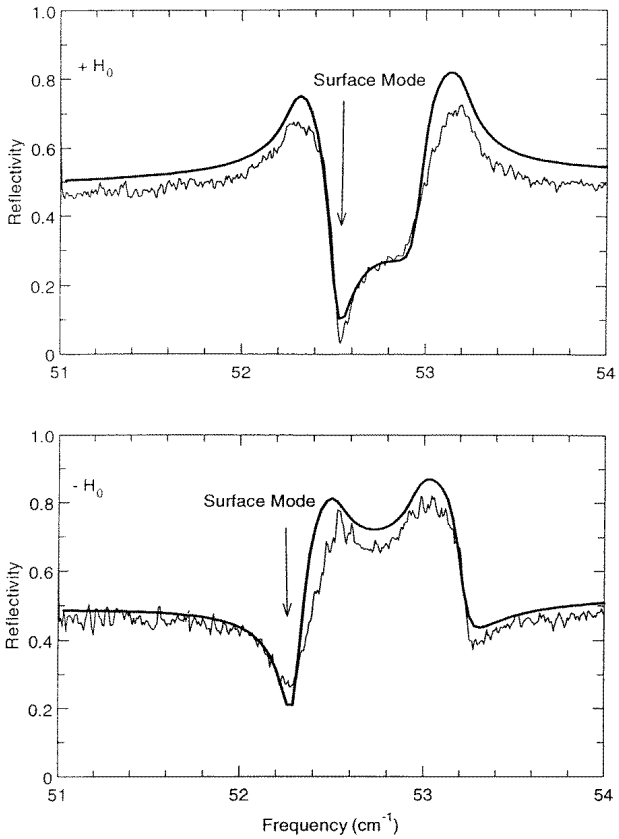

Figure 5. Experimental (thin line) and theoretical (thick line) ATR spectra of FeF_2 with the easy axis parallel to the applied field. $T = 1.7$ K and the resolution is 0.02 cm^{-1}; (top panel) $H_0 = +0.3$ T and (bottom panel) $H_0 = -0.3$ T.

with the applied field in the opposite direction. This is a unique effect in the far infrared. Comparing the shape of the features obtained using ATR to those in the reflectivity spectra, it is clear that the sharp dips in the ATR spectra are due to surface features, and they have also clearly moved to a higher frequency and are no longer within the bulk bands. Such spectra can of course only be obtained with the enhancement in the wave vector introduced by the prism. Both ATR spectra show weak interaction at the middle bulk band. For $+H_0$ the bulk band is seen as a shoulder on the rising edge after the surface polariton dip, and for $-H_0$ the bulk band is seen as a weak, but typical, bulk dip. The non-reciprocity of the upper bulk band seen in the spectra is attributed to another surface resonance just inside the upper bulk band for $H_0 = -0.3$ T, and this surface feature only exists on one side of the dispersion curve. We believe that this is the first observation of the virtual surface mode in antiferromagnets. Again the theoretical fits are in excellent agreement with experiment. A similar analysis has been carried out for all measured spectra.

The experimental dispersion curves (figure 6) are plotted with the combined data extracted from careful interpretation of the results of oblique-incidence reflectivity studies and the ATR measurements using all three prisms. In addition to the ATR measurements with a near-optimum ATR gap for coupling to the surface excitations, many of the experiments

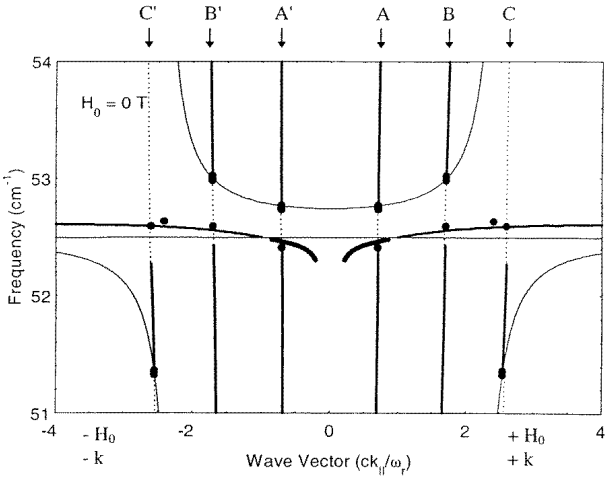

(a)

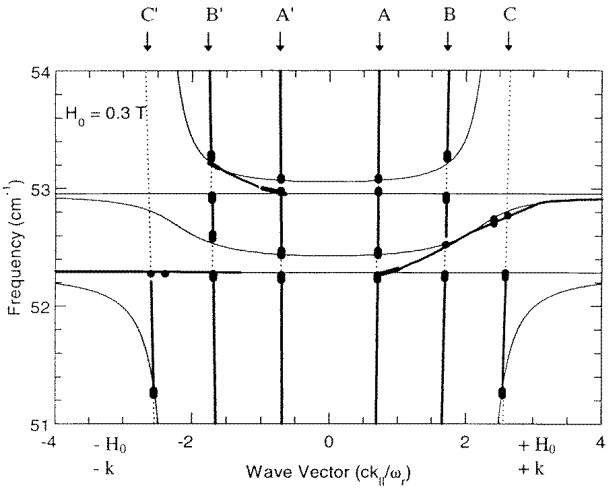

(b)

Figure 6. Experimental and theoretical dispersion curves for (a) $H_0 = 0$ T, (b) $H_0 = \pm 0.3$ T and (c) $H_0 = \pm 6$ T. The experimental points are marked by the spots and the solid, nearly vertical lines. Theoretical bulk regions (thin lines) and surface modes (thick lines) are calculated for zero damping. The surface resonances (very thick lines) are calculated with a damping parameter of 0.05 cm^{-1}. The dotted lines represent the theoretical scan lines. The reflectivity scan lines A and A′ are for an angle of incidence of 45°. B, B′ and C, C′ are the ATR scan lines for angles of incidence of 30° and 50°, respectively. ATR data obtained with an angle of incidence of 45° are shown between the 30° and 50° scan lines. The other parameters are as in figure 2.

were repeated with a minimum gap, thus enhancing the bulk coupling to allow more accurate measurements of the bulk edges. Dispersion curves for zero applied field, for a weak applied field (± 0.3 T) and for a relatively strong applied field (± 6 T) are presented. The thin solid lines mark the edges of the theoretical bulk continua calculated using the above parameters. In between the bulk continua, in the reststrahl regions, are the surface modes. For later reference we also plot the surface resonances, which exist only in the presence of damping.

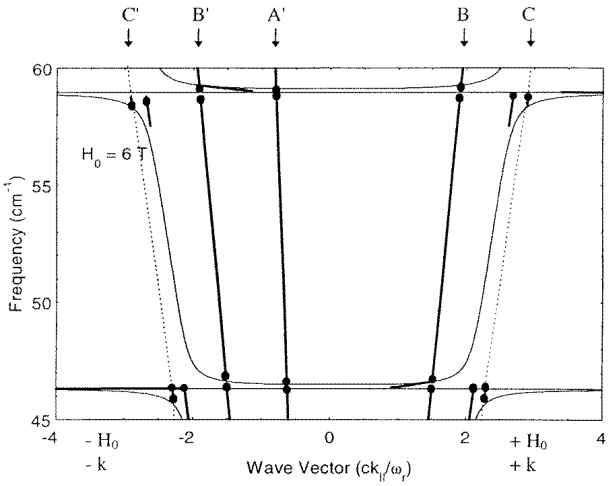

(c)

Figure 6. (Continued)

These are represented by the thick solid lines. The detailed derivation of the dispersion relations is given elsewhere. Each solid spot represents an experimental measurement and the thick nearly vertical straight lines indicate regions of reduced reflectivity indicative of bulk modes. The positions of these lines correspond to the scan lines determined by the scattering geometry. If the edge of a bulk band could not be unambiguously identified, usually due to the mixing of modes, this is indicated by solid lines which do not end in an experimental spot. Single spots with no line attached are measurements of surface modes. The uncertainty of the bulk edges is estimated to be about ± 0.05 cm^{-1}, and the uncertainty is less for the sharper surface features. This uncertainty is due to the difficulty of accurately determining the bulk edges due to the presence of magnon damping. It, therefore, does not indicate inaccuracies in the experimental spectra and is not caused by insufficient experimental resolution. The uncertainty is depicted in the figures by the approximate size of the experimental spots.

Figure 6(a) is a plot of the dispersion curves in the absence of an external field. They are of course reciprocal for both bulk and surface features. Due to the mixing of modes it was not possible to accurately determine the upper edge of the lower bulk band; however, the positions of the surface resonances and the bulk continua are in good agreement with theory. Note that the calculated dispersion curves with the exception of the surface resonance have been calculated with negligible damping; however, since the surface resonances are clearly visible in the experimental spectra they have been included for easy comparison of the spectra to the dispersion curves.

Applying a weak external field, figure 6(b), causes the two bulk regions seen for $H_0 = 0$ to separate in frequency and an additional bulk band is observed in the reststrahl region separating the lower and upper bulk bands. It is clear that the bulk regions remain reciprocal with an applied field despite the inevitable magnon damping. The surface modes, however, are strikingly non-reciprocal. The surface polariton curve for propagation in the $-\boldsymbol{k}_{\parallel}$ direction shifts to a lower frequency towards the lower bulk band while the surface curve for propagation in the $+\boldsymbol{k}_{\parallel}$ direction moves up in frequency. Similarly the surface resonances display non-reciprocity to be discussed in more detail in the following section.

The effect of a relatively strong applied field is shown in figure 6(c). Again the upper and lower bulk regions separate and the middle bulk band widens. The surface modes now lie along the edges of the bulk bands and can no longer be resolved experimentally.

3. Surface resonances

As has been pointed out, the surface polaritons propagating on an antiferromagnet can be strongly non-reciprocal in the presence of a magnetic field. In contrast, bulk magnetic polaritons in an infinitely extended medium are reciprocal. It is therefore somewhat surprising that there can be strong non-reciprocity in the reflectivity when the frequency is in the range where bulk modes propagate. One possible explanation for this non-reciprocity is that damped surface modes, or surface resonances, may exist inside the bulk band. Since these resonances are surface excitations, they retain the non-reciprocity of the true surface modes.

Surface resonances in antiferromagnets have been discussed previously in the literature [19]. In the absence of damping, one can find surface wave-like solutions to Maxwell's equations and boundary conditions where the electric and magnetic fields are all proportional to $\exp(\mathrm{i}(kx - \omega t))\exp(-\alpha y)$ in the antiferromagnet. In the vacuum above the antiferromagnet we have solutions which are proportional to $\exp(\mathrm{i}(kx - \omega t))\exp(+\beta y)$. Here ω is a real frequency, and k and α are also real. When damping is included the original solution must be modified slightly. For example one can choose ω to be real, and α, β and k complex†. Such a solution represents a dissipative wave with an attenuation along the surface governed by the imaginary part of k. Similarly the real part of α governs the exponential decay of the wave as it penetrates into the antiferromagnet while the imaginary part of α indicates the oscillatory behaviour in the y-direction. Initially we require both α and β to have positive real parts in order to ensure exponential decay of the surface wave as one moves away from the interface. We will eventually discuss when this condition may be relaxed slightly in order to find slightly different surface resonances.

We have already discussed the observed sharp dips in the reflectivity spectra shown as figures 2 and 3, and can now identify these dips as surface resonances. This is also in agreement with the above dispersion curves, and it is clear that the sharp dips observed in the spectra occur at the frequencies where the calculated surface resonances cross the reflectivity scan line. As mentioned, the surface modes penetrate into the bulk bands in a non-reciprocal way, i.e. the surface mode on the $+\boldsymbol{k}$ side penetrates into the lower bulk band while the surface mode on the $-\boldsymbol{k}$ side does not. Similarly, the high-frequency surface mode on the $-\boldsymbol{k}$ side now crosses the light line. There is no equivalent mode on the $+\boldsymbol{k}$ side. It can be seen that when damping is absent, the surface dispersion curves do not cross the light line for the incident radiation. As a result, the reflectivity does not measure these non-reciprocal surface features and is essentially reciprocal. With the increase in damping, surface resonances appear which do cross the light line. The crossing on the $+\boldsymbol{k}$ side produces the low-frequency dip in the reflectivity, and the crossing on the $-\boldsymbol{k}$ side produces the high-frequency dip.

In the absence of damping the high-frequency surface mode on the $-\boldsymbol{k}$ side has an upper bound when the surface mode intersects the bulk band. This mode does not appear to extend significantly further upwards when damping is introduced if we restrict the solutions to the exponential decay required by imposing $\mathrm{Re}\,\alpha > 0$ and $\mathrm{Re}\,\beta > 0$. However, it is

† It is also possible to choose k to be real, and ω and α complex. For the modes discussed here, the essential results—the extension of those for the surface modes—are effectively the same.

possible to examine situations where we choose $\mathrm{Re}\,\alpha < 0$ and $\mathrm{Re}\,\beta > 0$. This is appropriate only in the case where $\mathrm{Re}\,\alpha$ is small, and so the exponential increase in the wave as one moves away from the surface into the antiferromagnet is small. This is, in fact, just the situation where the $-\boldsymbol{k}$ surface mode intersects the bottom of the upper bulk band, since this is where $\mathrm{Re}\,\alpha = 0$. As a result, we can find a damped surface mode inside the upper bulk band as well. We note that there is no equivalent mode on the $+\boldsymbol{k}$ side of the dispersion relation. Mathematically there is a solution for modes on $+\boldsymbol{k}$, but they are non-physical. The $+\boldsymbol{k}$ modes do not intersect the upper bulk band and therefore they do not obey the condition that $\mathrm{Re}\,\alpha$ is very small.

The high-frequency surface resonance seems to be measured in the 30° ATR experiment. When we look at the $-H_0$ ATR curve, we see a sharp drop near the frequency of the upper surface resonance. The $+H_0$ ATR curve shows no sharp dip, but a broad decrease.

4. Independent determination of the anisotropy and exchange fields

In the earliest experiments [16] on FeF_2, only the resonance frequency

$$\omega_r = \gamma(2H_A H_E + H_A^2)^{1/2}$$

was found directly from far-infrared measurements. To obtain independent values for H_A and H_E it was necessary to introduce transverse susceptibility data from other experiments. We show in this section that one can obtain reasonable measures of H_A, H_E and M_S solely from far-infrared reflectivity measurements.

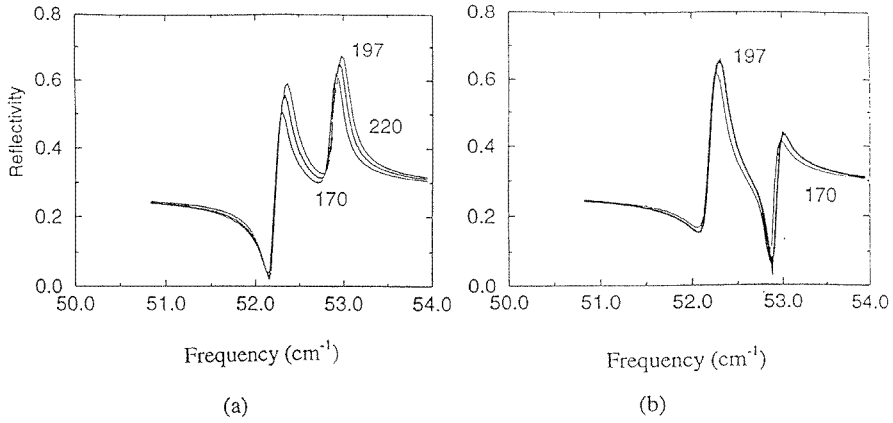

Figure 7. An illustration of how different values of H_A lead to very similar spectra provided that the resonance frequency is kept constant. The applied fields are (a) 0.3 T and (b) −0.3 T.

On the basis of the excellent fits between theory and experiment shown in the previous section, one might expect that independent values for the exchange and anisotropy fields could be obtained simply by comparing theory and experiment for a single geometry, s-polarized reflectivity, where the easy axis is parallel to the applied field and the plane of incidence is perpendicular to the applied field. In fact, if M_S is known or can be deduced, as is often the case at low temperatures in bulk samples, independent values for H_A may be obtained with an accuracy of about 15%. This is illustrated in figure 7 where we show different theoretical reflectivity curves for different values of H_A, with the resonance field

ω_r held constant. The shifts in frequency for the different cases are within the experimental resolution.

At higher temperatures or for thin films, M_S may not be known. In this case, it is unfortunately possible to obtain quite reasonable fits to the data with enormous variations in H_A. The reason for this is the following. In the previous reflection geometry with the easy axis parallel to the applied field the permeability tensor has the form

$$\boldsymbol{\mu} = \begin{pmatrix} \mu_{xx} & \mu_{xy} & 0 \\ \mu_{yx} & \mu_{yy} & 0 \\ 0 & 0 & \mu_{zz} \end{pmatrix}. \tag{1}$$

The individual components are given by

$$\mu_{xx} = 1 + 4\pi\gamma^2 H_A M_S(\Upsilon^+ + \Upsilon^-) \tag{2}$$

$$\mu_{xy} = -\mu_{yx} = \mathrm{i}\,4\pi\gamma^2 H_A M_S(\Upsilon^+ - \Upsilon^-) \tag{3}$$

with

$$\Upsilon^{\pm} = [\omega_r^2 - (\omega \pm \gamma H_0)^2]^{-1}. \tag{4}$$

We see that H_A and M_S always appear as a product. Because of this it is possible to get very good matches to the experimental data with quite different parameters. Basically any deviation from the true value of H_A can be balanced by a change in M_S and vice versa.

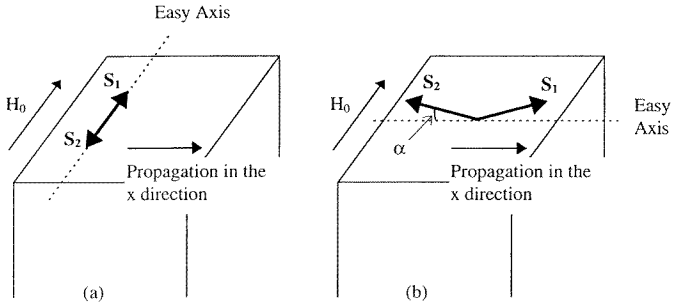

Figure 8. (a) The initial configuration. The crystal is placed with the easy axis parallel to the applied field and the spins, $\boldsymbol{S}_1$ and $\boldsymbol{S}_2$, align along the field. (b) The new configuration. The crystal is placed with the easy axis perpendicular to the applied field. This causes the spins $\boldsymbol{S}_1$ and $\boldsymbol{S}_2$ to cant towards the applied field. The canting angle is α.

It is obviously of interest to look at other geometries [20] so as to obtain additional information. Earlier theoretical work has shown that in the transverse geometry, where the external magnetic field is perpendicular to the easy axis, the permeability tensor still has the form given in equation (1). However, the individual components are now given [21] by

$$\mu_{xx} = 1 + 8\pi\gamma^2 M_S H_0 \sin\alpha/(\omega_\perp^2 - \omega^2) \tag{5}$$

$$\mu_{xy} = \mathrm{i}\,8\pi\gamma M_S \omega \sin\alpha/(\omega_\perp^2 - \omega^2) = -\mu_{yx} \tag{6}$$

$$\mu_{yy} = 1 + 8\pi\gamma^2 M_S(H_0 \sin\alpha + H_A \cos 2\alpha)/(\omega_\perp^2 - \omega^2) \tag{7}$$

$$\mu_{zz} = 1 + 8\pi\gamma^2 M_S H_A \cos^2\alpha/(\omega_\parallel^2 - \omega^2). \tag{8}$$

In these equations α is the canting angle, measured from the x-axis, induced by the applied field (figure 8). This angle is given by the equation

$$\sin\alpha = \frac{H_0}{H_A + 2H_E}. \tag{9}$$

There are two important resonance frequencies. The first resonance

$$\omega_\perp = (\omega_r^2 \cos^2\alpha + 2\gamma^2 H_0 H_E \sin\alpha)^{1/2} \tag{10}$$

is common to the upper block of the permeability tensor. These terms are probed in a reflectivity experiment with s-polarized radiation where the plane of incidence is parallel to the easy axis. Similarly there is a second resonance

$$\omega_\parallel = \omega_r \cos\alpha \tag{11}$$

which occurs in the μ_{zz}-permeability. This resonance is seen in a p-polarized reflectivity measurement.

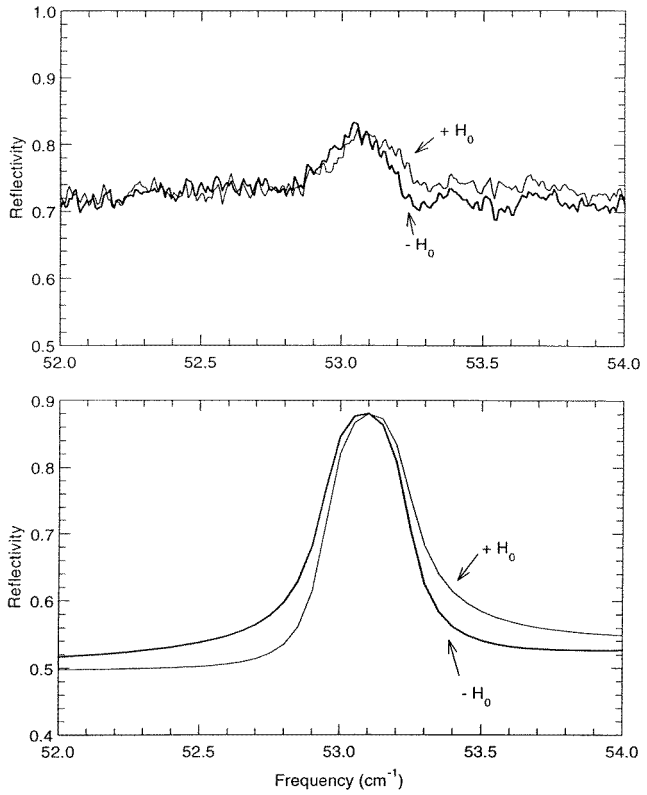

Figure 9. Experimental (top panel) and theoretical (bottom panel) ATR spectra of FeF_2 with the easy axis perpendicular to the applied field. The experimental parameters are: $H_0 = \pm 6$ T, gap $= 17$ μm and $\theta = 30^\circ$. The spectra demonstrate slight non-reciprocal behaviour. The theory was calculated using the parameters of figure 1.

One might think that since the resonance frequency is shifted with applied field, the reflectivity curve essentially shifts with it. In this case one can obtain explicit expressions for the anisotropy field:

$$H_A = \frac{\omega_r^2}{\gamma^2 H_0}\sqrt{1 - \left(\frac{\omega_\parallel}{\omega_r}\right)^2} \tag{12}$$

which is appropriate for p-polarization measurements, and

$$H_A = \frac{\omega_r}{\gamma^2 H_0}\sqrt{\frac{\omega_r^2 + (\gamma H_0)^2 - \omega_\perp^2}{2}} \tag{13}$$

which is appropriate for s-polarization measurements. By measuring ω_r in zero field, and $\omega_\parallel$ and $\omega_\perp$ with a large external field one can obtain useful estimates for H_A. Having H_A, one can then easily find H_E and M_S through the equation for ω_r and the usual reflectivity measurements in the geometry of figure 8(a). There are, however, a number of problems using this approach directly.

(1) The s-polarization shift in the resonance frequency is reasonable (0.26 cm^{-1} at 6 T), but the signal in the reflectivity is rather weak: typically the change in reflectivity is of the order of 5% for low temperatures and significantly smaller at higher temperatures. This means that noise can significantly influence the result.

(2) The p-polarization shift in the resonance frequency is small (0.057 cm^{-1} at 6 T), but the change in the reflectivity is significantly larger, 60%, which compensates somewhat.

These problems can be overcome by using ATR reflectivity in s polarization. This maintains the larger frequency shifts in s polarization, but increases the change in the reflectivity to about 25%.

Unfortunately, the assumption that the reflectivity curve simply shifts in frequency according to the shift in the resonance position is not quite true. There is a slight non-reciprocity in the frequency shift depending on the sign of the applied field. This is illustrated in figure 9 where we show ATR reflectivity spectra for s-polarized radiation at various different fields. In addition to the non-reciprocal shifts discussed above, there can also be some slight frequency shift due to misalignment of the crystal. Without great care, we estimate that the error in the estimates for H_A can be of the order of 15–25%.

5. Summary

In this paper we have described in detail the measurements carried out which led to experimentally determined dispersion curves for the antiferromagnet FeF_2. We have shown how the dispersion relations change from being reciprocal in the absence of an applied field to demonstrating a striking non-reciprocal behaviour in the presence of an applied field. By tracking the movement of the surface and bulk polaritons with various applied fields we demonstrate how the observed non-reciprocity can be controlled by the field. We also show how the non-reciprocity observed in the reflectivity experiments is caused by the presence of surface resonances which are only seen in the presence of damping. These modes extend from the pure surface modes which exist in the reststrahl bands into the bulk regions, which explains the non-reciprocity observed at the frequencies of bulk propagation. All of the experimental spectra are in excellent agreement with theory. We have also described how far-infrared experiments alone can provide independent measurements of some of the material parameters controlling the spin system.

Acknowledgments

MRFJ, SAF and REC are supported by the EPSRC. This work is part of a general programme for far-infrared investigations of magnetic systems supported by the EPSRC through Grants No GR/G54139 and No GR/J90831. REC was also supported by US ARO Grant No DAA H04-94-G-0253

References

[1] Grunberg P 1989 *Light Scattering in Solids V* ed M Cardona and G Guntherodt (Berlin: Springer)
[2] Patton C E 1984 *Phys. Rep.* **103** 251
[3] Hillebrands B and Guntherodt G 1993 *Ultrathin Magnetic Structures II* ed J A C Bland and B Heinrich (Berlin: Springer)
[4] Windsor C G and Stevenson R W H 1966 *Proc. Phys. Soc.* **87** 501
[5] Bell R J 1972 *Introductory Fourier Transform Spectroscopy* (New York: Academic)
[6] Lagois J and Fischer B 1976 *Phys. Rev. Lett.* **36** 680
[7] Yang F, Sambles J R and Bradberry G W 1990 *Phys. Rev. Lett.* **64** 559
[8] Dumelow T, Parker T J, Smith S R P and Tilley D R 1993 *Surf. Sci. Rep.* **17** 151
[9] Camley R E 1987 *Surf. Sci. Rep.* **7** 103
[10] Sanders R W, Belanger R M, Motokawa M and Jaccarino V 1981 *Phys. Rev.* B **23** 1190
[11] Remer L, Lüthi B, Sauer H, Geick R and Camley R E 1986 *Phys. Rev. Lett.* **56** 2752
[12] Brown D E, Dumelow T, Parker T J, Kamsul Abraha and Tilley D R 1994 *Phys. Rev.* B **49** 12 266
[13] Dumelow T, Brown D E and Parker T J 1993 *18th Int. Conf. on Infrared and Millimeter Waves (Colchester); Proc. SPIE* **2104** 633
[14] Jensen M R F, Parker T J, Kamsul Abraha and Tilley D R 1995 *Phys. Rev. Lett.* **75** 3756
[15] Jensen M R F, Feiven S A, Parker T J and Camley R E 1997 *Phys. Rev.* B **55** 2745
[16] Ohlmann R C and Tinkham M C 1961 *Phys. Rev.* **123** 425
[17] Camley R E and Mills D L 1982 *Phys. Rev.* B **26** 1280
[18] Shu C and Caille A 1982 *Solid State Commun.* **42** 233
[19] Stamps R L and Camley R E 1989 *Phys. Rev.* B **40** 596
[20] Kamsul Abraha and Tilley D R 1996 *Surf. Sci. Rep.* **24** 129
[21] Almeida N S and Mills D L 1988 *Phys. Rev.* B **37** 3400